ELSEVIER

Quaternary Science Reviews 25 (2006) 1039–1052

QSR

Evidence for multiple paleomagnetic intensity lows between 30 and 50 ka BP from a western Equatorial Pacific sedimentary sequence

Cécile L. Blanchet*, Nicolas Thouveny, Thibault de Garidel-Thoron

Centre Européen de Recherche et d'Enseignement en Géosciences de l'Environnement (CEREGE), CNRS-Université Paul Cezanne, Europôle Méditerranéen de l'Arbois, BP 80, 13545 Aix en Provence Cedex 04, France

Received 23 April 2004; accepted 19 September 2005

Abstract

A paleomagnetic study was carried out on the radiocarbon dated MD97-2134 core located in the western Equatorial Pacific (Southern Papua New Guinea margin). Rock magnetic investigations revealed changes of the magnetic mineralogy along the hemi-pelagic sedimentary sequence but the reconstruction of past direction and relative paleointensity variations of the geomagnetic field remained feasible. Four successive paleointensity drops are recorded between 30 and 50 ka BP. The largest one is associated with an abrupt swing of declination and inclination interpreted as a smoothed signature of the Laschamp excursion (~41 ka BP). The succession of four events of weak intensity between 30 and 50 ka BP introduces a complex behaviour of the geomagnetic field in the time interval spanning over the Laschamp and the Mono Lake excursions.

1. Introduction

High-resolution records of the paleomagnetic field provide a series of markers applicable for global scale correlation of paleoclimatic archives. The interval 30–50 ka BP containing important evidence of the variability of the climate during Marine Isotope Stage (MIS) 3 deserves more detailed investigations. The present debate about the Mono Lake and the Laschamp excursions and their respective age illustrates this point. Quasi-reversed magnetizations measured in the Laschamp and Olby lavas (Chaîne des Puys, France) introduced the concept of rapid incomplete reversals (Bonhommet and Babkine, 1967). First dated between 20 and 8 ka BP (Bonhommet and Zahringer, 1969), these lavas later provided K/Ar ages between 40 and 50 ka BP (e.g. Gillot et al., 1979). The excursion was later shown to be associated with weak paleointensities (Roperch et al., 1988). Studies of Maar lake sediments of Lac du Bouchet and Lac St Front (Thouveny et al., 1990, 1993; Vlag et al., 1996) demonstrated that wide departures of the virtual geomagnetic pole occurred near 37 ka BP (33 ka ^{14}C BP) during the period of weakest relative paleointensities (RPI). Marine sediments RPI and directional records also helped to better constrain the age of the Laschamp excursion. By correlating a North Atlantic Paleointensity stack (NAPIS) (Laj et al., 2000) to the cosmonuclide ^{36}Cl record of the GRIP ice-core, Wagner et al. (2000) constrained the age of the low RPI event at ~41 ka BP. The excursion, the low RPI event and the associated ^{10}Be overproduction are recorded 30 cm beneath the signature of Heinrich Event 4 in the Portuguese margin sedimentary sequence, at an interpolated age of ~41 ka BP (Carcaillet et al., 2004; Thouveny et al., 2004). These estimates agree with the mean age 40.4 ± 2 ka computed from Ar/Ar and K/Ar datings of the Laschamp and Olby lava flows (Guillou et al., 2004).

The occurrence of the excursion beyond the European and North Atlantic area was attested by directional anomalies and RPI minima recorded in sedimentary sequences from the southern Atlantic Ocean (Channell et al., 2000) and the southern Indian Ocean (Mazaud et al., 2002).

Studies of lacustrine sequences of the western United States have provided fundamental data about excursions. The Mono Lake excursion was first described in

*Corresponding author. Tel.: +33 4 42 97 15 81; fax: +33 4 42 97 15 95.
E-mail address: blanchet@cerege.fr (C.L. Blanchet).

0277-3791/$ - see front matter © 2005 Elsevier Ltd. All rights reserved.
doi:10.1016/j.quascirev.2005.09.001

sedimentary outcrops from the Mono Lake Basin, California (Denham and Cox, 1971; Liddicoat and Coe, 1979), and later found in other lake sequences from the same region: Summer Lake (Negrini et al., 1984) and Lake Lahontan (Liddicoat, 1992; Liddicoat, 1996). Preliminarily dated at ~24 ka BP (Denham and Cox, 1971), this excursion was recently re-dated at ~32 ka BP (Benson et al., 2003) and associated with a low RPI event located at ~32 ka BP in the ^{36}Cl record of the GRIP ice-core (Wagner et al., 2000).

The ash layers of Wilson Creek at Mono Lake Basin were recently dated to the interval ranging from 38 to 41 ka BP (Kent et al., 2002). This timing and the absence of a second excursion in the Wilson Creek Formation suggested that the excursion recorded at Mono Lake is actually correlative with the Laschamp excursion. However, at Summer Lake, two distinct excursions are recorded (Negrini et al., 2000; Zic et al., 2002).

Finally, both the NAPIS (Laj et al., 2000) and the GRIP cosmogenic isotope records (Wagner et al., 2000) suggest that two distinct geomagnetic dipole moment lows occurred between 30 and 45 ka, supporting the distinction of the Mono Lake and Laschamp excursions.

This non-exhaustive review of the evidence for the Laschamp and Mono Lake excursions indicates that data about paleomagnetic field changes during the 30–50 ka BP interval are needed, especially from widely distributed regions. Here, we present new paleomagnetic results obtained from a sedimentary core (MD97-2134) collected on the southern margin of Papua New Guinea, in the West Equatorial Pacific, a region where paleomagnetic variations are poorly documented.

2. Geographical setting and core description

The MD97-2134 core (Fig. 1) was retrieved southeast of the Papua New Guinea margin (Lat. 09°54.44S; Long. 144°39.65E, 760 m depth). The core, 26.9 m long, was collected using the Calypso corer of the French R.V. Marion Dufresne during the IMAGES III campaign (1997).

Beneath 2 m of oxidized biogenic carbonate ooze, the sediments consist of green-grey hemi-pelagic clays. Iron diagenesis is revealed by the presence of iron sulphide (pyrite) and iron phosphate (vivianite) patches. Two thick tephra layers are identified between 6.3 and 6.8 m and between 15 and 15.3 m with sharp magnetic signatures. Other thinner tephra layers are located at 8.3 and 13.25 m. The depth scale was corrected for two voids caused by gas expansion.

3. Methods

After 4 years of storage in a cold room, the core was subsampled using U-channels (length = 1.5 m; section = 2 × 2 cm) and using standard 8 cm^3 cubes of plastic pushed into the sediment at regular intervals, in order to obtain: (i) a low-resolution record (80 cm intervals) of the anisotropy of susceptibility, and (ii) a high-resolution subsampling (2 cm intervals) for the analysis of natural remanent magnetization (NRM) within selected depth intervals.

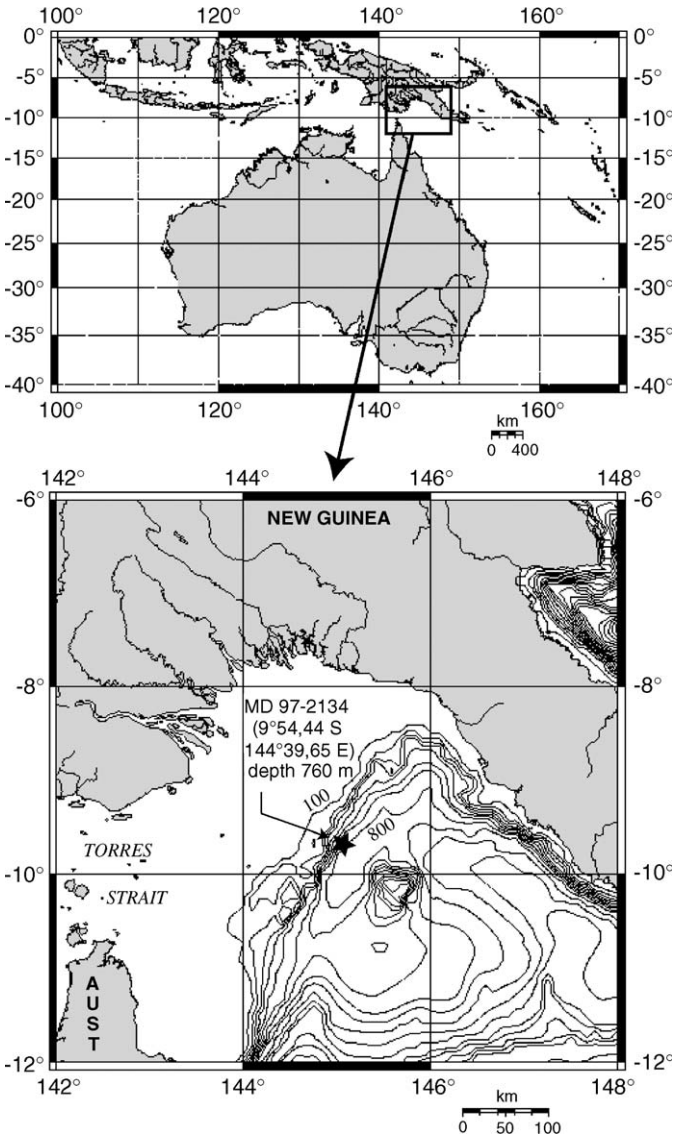

Fig. 1. Geographical location of the Ashmore Trough and Core MD97-2134 (star). The bottom panel presents the bathymetric map of the coring site area and the relation with the coast line and the Fly river delta. Intervals of bathymetric contours are 100 m.

The magnetic susceptibility (MS) was measured on U-channels samples using a Bartington MS2B probe. The anisotropy of MS was analysed on the cubic samples using a Kly 2 Kappabridge.

Hysteresis loops and demagnetization curves of the saturation isothermal remanent magnetization (SIRM) were analysed on selected microsamples using a VSM Micromagnetometer (P.M.C., model 3900).

Natural and artificial remanent magnetizations were measured on a three axis direct current SQUID

magnetometer (2G model 760R) with response curves of, respectively, ~4 cm (for the X and Y axes) and ~6 cm (for the Z axis); this procedure of pass-through measurement implies a slight smoothing of the signal continuously measured on U-channels.

The NRM was measured every 2 cm on U-channels collected along the core and on additional discrete samples. The alternating field (AF) demagnetization was imposed at successive steps [5, 10, 15, 20, 25, 30, 40, 60 and 80 mT] on U-channels and standard specimens. Stepwise thermal demagnetization was imposed at 100, 160, 220, 280, 340, 400 and 500 °C on standard specimens dried in zero field at ambient temperature.

Anhysteretic remanent magnetization (ARM) imparted on U-channels in a 100 mT AF and a 0.1 mT steady field, was measured and demagnetized according to the same AF demagnetization process as the NRM.

Isothermal remanent magnetization (IRM) was imparted in a 1 T direct field ($IRM_{1\,T}$) and a 0.3 T backfield ($IRM_{-0.3\,T}$) by passing U-channels through permanent rare earth magnets (Rochette et al., 2001). In order to study the IRM acquisition, discrete specimens were submitted to stepwise increasing fields from 0 to 3 T on a pulse magnetizer. The IRM acquired at 3 T, called here saturation IRM (SIRM), was then stepwise demagnetized up to 650 °C in an Argon atmosphere.

4. Rock magnetic results

The magnetic susceptibility variations and the natural or artificial magnetizations intensity variations (Fig. 2) present a few notable features: (1) high ARM and NRM intensities at ~2.5 m; i.e. near the lithological transition between clays and carbonates, (2) large MS and IRM_0 spikes at the tephra layers and (3) a low MS and low magnetization intensity interval (zone A) defined by sharp boundaries at 8.8 and 11.8 m. AF demagnetization of IRM, ARM and NRM indicate that unblocking fields strongly vary along the sequence (Fig. 2). Such variations are also documented by normalized magnetic parameters (Fig. 3) and indicate changes of the magnetic mineralogy and/or magnetic grain size along the core. Magnetic susceptibility, K (Fig. 3a) is mostly influenced by large ferrimagnets such as coarse (Titano-) magnetite. The $IRM_{1\,T}$ is dominantly carried by (Ti-) magnetite and secondarily influenced by high-coercivity minerals, i.e. hematite or goethite. ARM is mostly carried by (Ti-) magnetite; its unblocking field varies with the grain size of this fraction. Therefore, if (Ti-) magnetite is the only contributing ferrimagnetic mineral, the $ARM_{30\,mT}$/ARM ratio (Fig. 3c) constitutes a proxy of the ARM medium destructive field (ARM_{MDF}) which in turn can be considered as a proxy of the relative grain size of the (Ti-) magnetite fraction.

In summary, transitions from low to high, or high to low ratios correspond to a decrease, or an increase of the magnetite grain size. In the same conditions of (Ti-) magnetite dominance, ARM/SIRM (Fig. 3b) and SIRM/K (Fig. 3d) are inversely related to the magnetic grain size: low ratios indicate large grain sizes as high ratios indicate small. Such inferences cannot be drawn when other ferrimagnetic minerals such as greigite (Fe_3S_4) and pyrrhotite (Fe_7S_8) are present. Indeed, Roberts (1995) showed that SIRM/K values of greigite are high; and Peters and Thompson (1998) demonstrated that (i) pyrrhotite is also characterized by large SIRM/K values and (ii) that both pyrrhotite and greigite significantly increase the $ARM_{30\,mT}$/ARM ratio.

Those considerations imply that if the magnetic fraction of the MD97-2134 was exclusively composed of (Ti-) magnetite, then the three magnetic grain size indicators (Fig. 3b–d) would present parallel variations along the sequence. However, this is clearly not the case, especially between 8 and 11 m (zone A) where ARM/SIRM and SIRM/K both decrease while $ARM_{30\,mT}$/ARM abruptly increases. This suggests that the magnetic fraction is a mixture of different ferrimagnetic minerals. This hypothesis can be checked using various coercivity parameters.

The hard IRM [$HIRM = 0.5\ (SIRM + IRM_{(-0.3\,T)})$] is the fraction of SIRM acquired above 0.3 T i.e. by high-coercivity minerals such as hematite, goethite or iron sulphides (Fig. 3e). The S ratio, [$-(IRM_{-0.3\,T})$/SIRM] is the ratio of the magnetization of low-coercivity minerals versus the total magnetization of all ferromagnetic minerals.

HIRM variations (Fig. 3e) present several minima at 7–8, 8.8–11.8 (zone A) and at 13.5–14.5 m, indicating low concentration of high-coercivity minerals. The strongly variable S ratio (Fig. 3f) reaches minimum values (0.65) in zone A, further indicating a diagenetic dissolution of the magnetite content.

Complementary information was drawn from hysteresis cycles obtained between −1 and 1 T (Fig. 4a–d) and from stepwise IRM acquisition up to 3 T (Fig. 4e and f). Hysteresis loops, after correction of para- or dia-magnetic contributions, generally indicate low saturation fields (<0.3 T) and low coercivities (Hc < 8 mT). Specimens of zone A have stronger Hc and Hcr (Hc > 10 mT and Hcr > 20 mT), indicated by wasp-waisted loops (Fig. 4c) and by a larger IRM increase above 0.3 T (Fig. 4f). Thermal demagnetization of SIRM was conducted up to 650 °C. In all cases, 95% of the SIRM is lost at 580 °C. Specimens of zone A are distinguished by a rapid loss of intensity between 240 and 400 °C that can be related, according to Roberts (1995), to the presence of greigite.

In summary, in zone A, magnetite dissolution is suggested by weak susceptibility and remanence values. The presence of ferrimagnetic iron sulphides is supported, despite weak SIRM/K values, by the: (1) drop of the S ratio, (2) increase of the remanence coercivity (up to 50 mT), (3) wasp-waisted hysteresis loops, (4) accentuated thermal demagnetization of the IRM between 240 and 400 °C and (5) abrupt increase of the ARM_{MDF} at the boundaries of zone A.

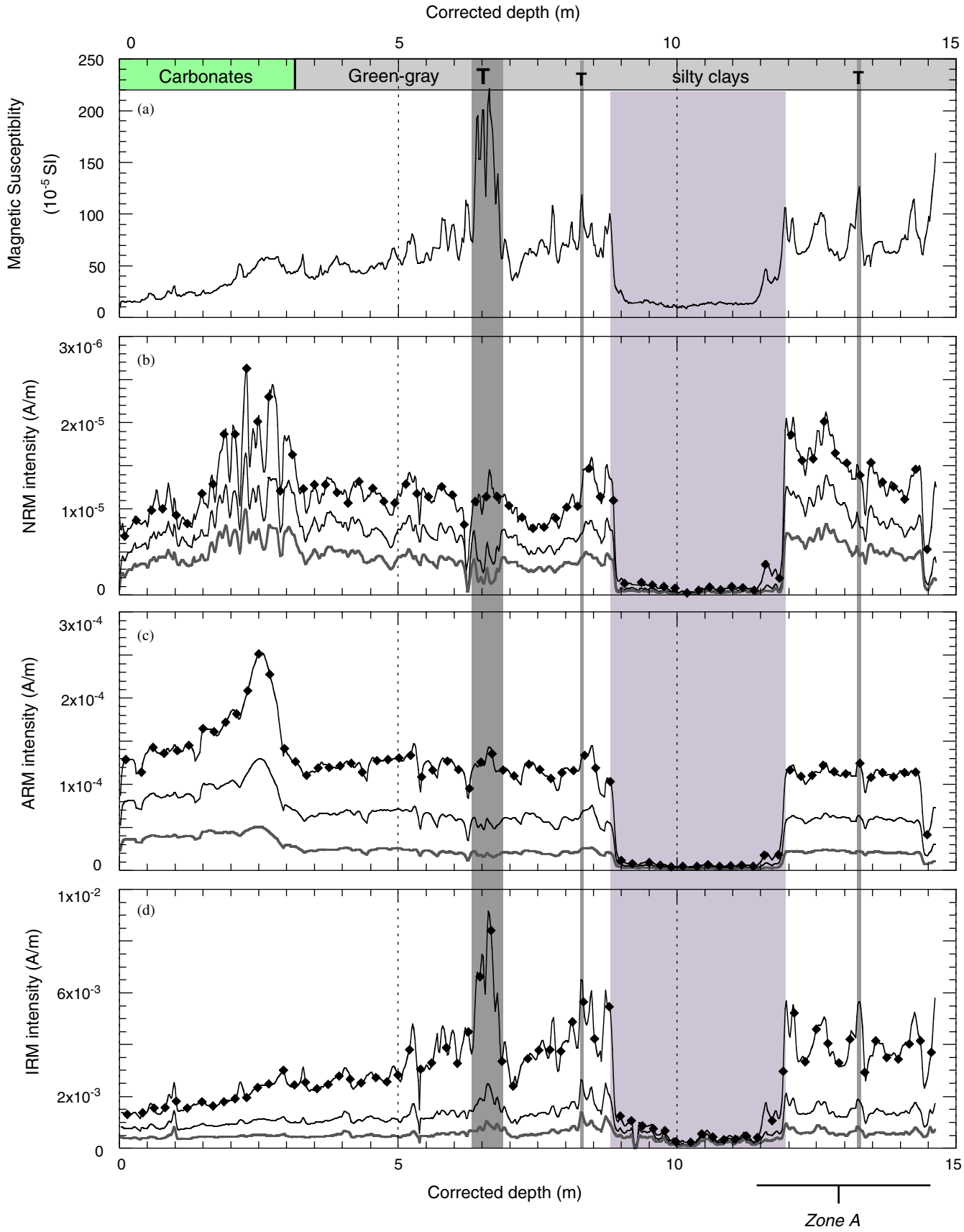

Fig. 2. Lithology, susceptibility and remanences plotted on the corrected depth scale (m) (i.e. after removal of the void lengths). Tephra layers are identified by T and grey bands. (a) Magnetic susceptibility (MS), (b) natural remanent magnetization (NRM), (c) anhysteretic remanent magnetization (ARM) and (d) isothermal remanent magnetization (IRM) intensities. Magnetizations are presented for 0, 20 and 40 mT AF steps. Zone A is underlined by a light-grey area.

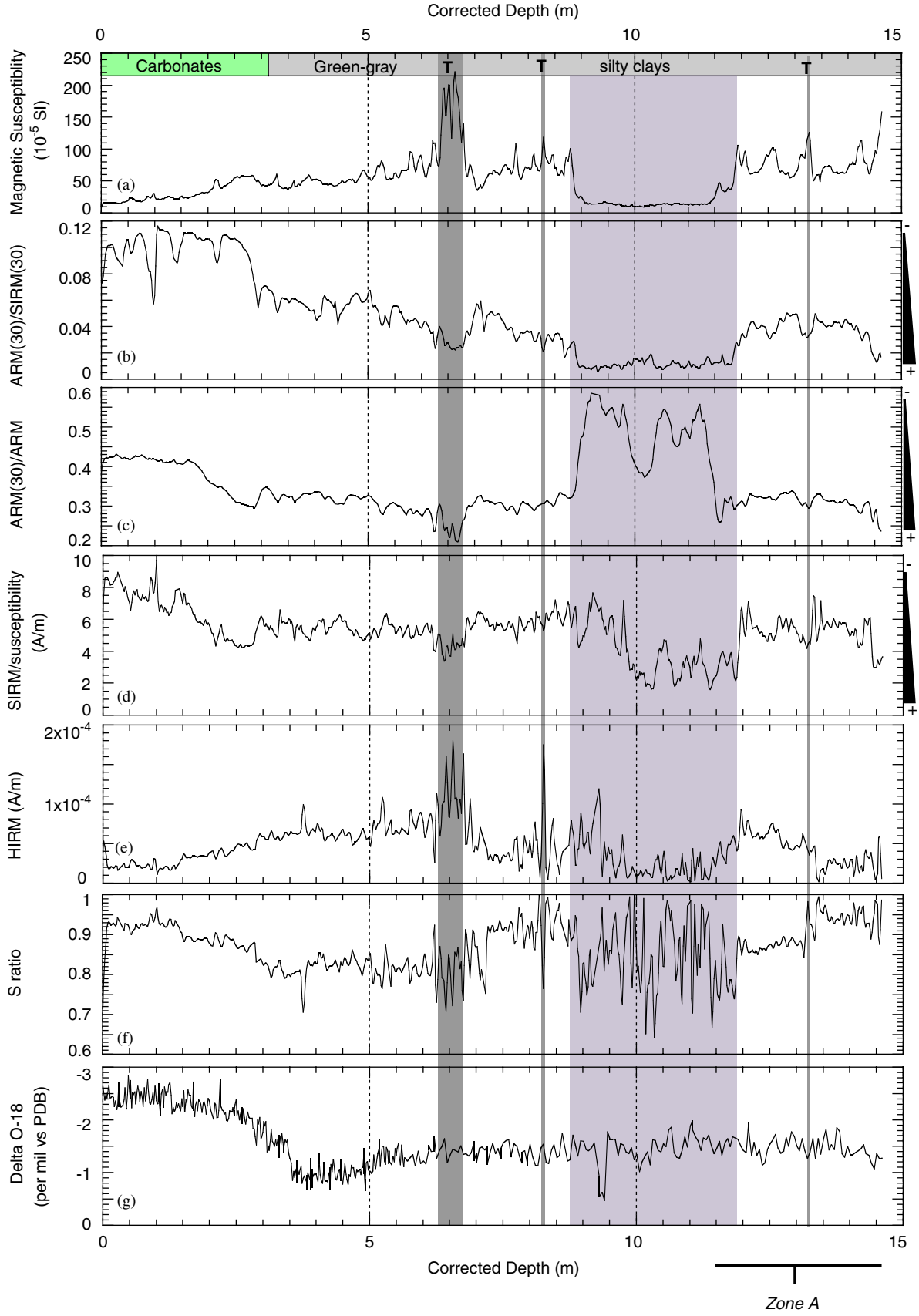

Fig. 3. Magnetic parameters and their ratios plotted on the corrected depth scale (m): (a) MS, (b) $ARM_{30\,mT}/SIRM_{30\,mT}$, (c) $ARM_{30\,mT}/ARM$, (d) SIRM/*K*, (e) HIRM, (f) *S* ratio and (g) $\delta^{18}O$ of the planktic foraminifera *Globigerinoides ruber*. Interpretation in terms of magnetic grain size is indicated on the right-side of the panels; note the contradictory information brought by the $ARM_{30\,mT}/ARM$. See details in the text.

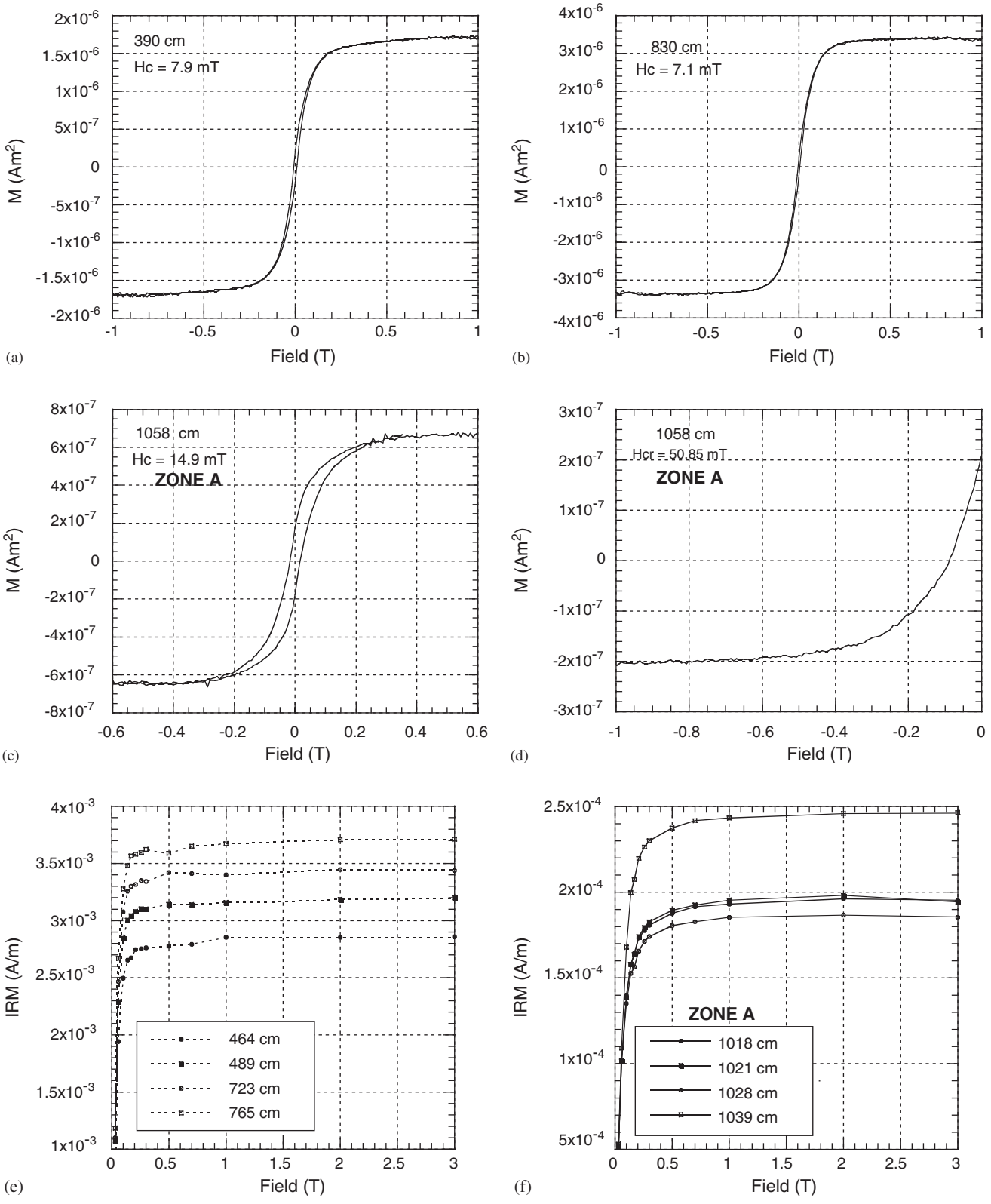

Fig. 4. Coercivity parameters: (a–c) hysteresis loops, (d) IRM demagnetization in reverse fields and (e, f) IRM acquisition up to 3 T. For zone A, note the higher coercivity and the wasp-waisted character of hysteresis cycle (c), high remanence coercivity (d) and high IRM saturation fields (f).

The MD97-2134 sedimentary sequence is affected by large changes of the magnetic fraction (nature, concentration and grain size) but these do not match with the first-order paleoclimatic information deducted from the classical $\delta^{18}O_{calcite}$ proxy record (Fig. 3g). Despite such variations, magnetic properties indicate that (Ti-)

magnetite is the main carrier of the NRM throughout the sequence, which allows to consider the paleomagnetic study as feasible.

5. Paleomagnetic results

5.1. Stability of intensity and direction magnetization

The medium destructive field (MDF) of the NRM lies between 25 and 30 mT in hemi-pelagic sediments and above 40 mT in sediments of zone A (Fig. 5a). A low unblocking field magnetization probably of viscous origin was removed below 10 or 15 mT; the characteristic remanent magnetization (ChRM) of selected pilot samples was thus computed on at least five directions obtained between 20 and 60 mT AF using the component analysis (Paleomac 5 software) (Cogné, 2003) (Fig. 5c–e). Thermal demagnetization performed on discrete specimens confirms the reliability of AF demagnetization (Fig. 5b and f–h). For U-channels, the direction of magnetization isolated at 20, 30 and 40 mT is compatible with the ChRM directions obtained on specimens (Fig. 6a and b), although the continuous measurement provides smoother declination and inclination profiles.

Most inclination values (Fig. 6a) range between -35° and -5°. The average inclination (-20°) is fully consistent with the inclination (-19.5°) of the field produced by an axial dipole at the site latitude. The inclination variation defines a regular paleosecular variation (PSV) of $\pm 15^\circ$ with maximum amplitudes in the interval 4–6 and 7–8 m. The signature recorded between 9.5 and 11.5 m is affected by a larger scatter between successive inclination values and characterized by the largest amplitude of the whole record (up to 40° between 10 and 10.5 m).

The declination curve (Fig. 6b) was constructed by adjusting declination patterns at the section boundaries. A correction of $\sim 50^\circ$ was imposed on the declination values in order to present declination curves centred on 0°. The most remarkable feature is a large amplitude swing (up to 70°) recorded between 10 and 10.5 m, affected by a larger scatter between successive declination values. This event corresponds to the anomaly described in the inclination curve.

The most intriguing feature of the directional record is the larger amplitude directional signature associated with larger noise. Stepwise AF and thermal demagnetization performed on specimens attest the stronger resistance of the magnetization (Fig. 5a and b) and the instability of its directions (Fig. 5h).

The anisotropy of magnetic susceptibility was measured in order to check the sedimentary fabric along the core (Fig. 7). Foliation dominates ($F < 8\%$, $L < 2\%$) everywhere (Fig. 7b). Down to 9 m, K_{max} inclinations range from 0° to 20°, and K_{min} inclinations generally range around 80° (Fig. 7c). In the 10–10.5 m interval, the scattered paleomagnetic directions are associated with K_{min} inclinations ranging from 55° to 75°. Since such weak bias does not constitute a clue for secondary sedimentary fabric due to sediment deformation, the scattered directions can be considered as the expression of geomagnetic direction anomalies linked with an abrupt secular variation or an excursion. However, it should be noted that the computed paleomagnetic pole co-latitudes do not exceed the conventional limit of 45°.

5.2. Estimation of the relative paleointensity variations

The use of normalized NRM intensity to evaluate RPI variations conventionally relies on the reliability criteria established by King et al. (1983) and further refined by Tauxe (1993). In the present case, hysteresis ratios, Hcr/Hc and Mr/Ms, suggest, as it is usually the case in sediment mixtures, that average grain size corresponds to the Pseudo-Single Domain range. It has to be emphasized, however, that such observation could also derive from a mixture of two populations of single domain and multi-domain grains.

The IRM_{max}/IRM_{min} ratio, index of ferromagnetic mineral concentration, presents large variations; the highest ratio (excluding the tephra layer) reaches ~20 at ~9 m and ~12 m. This is linked with the reduction and dissolution effects in the zone A sediments that led to a depletion in ferromagnetic minerals. Therefore, we can anticipate the unsuitability of the NRM normalization for reconstruction of the RPI variations across the boundaries of zone A.

The normalized parameters commonly used for deciphering RPI from sediments (NRM/K, NRM/SIRM and NRM/ARM) are presented in Fig. 6. Conventionally, the co-variation of these three parameters is a prerequisite for their use as RPI indicators (Tauxe, 1993).

NRM/K (Fig. 6d) and NRM/SIRM (Fig. 6e) present similar behaviours, both strongly different from the NRM/ARM profile (Fig. 6c). In the upper part, NRM/K and NRM/SIRM regularly decrease in relation with increasing trends of K and SIRM. In the lower part, and specifically across the boundaries of zone A, both exhibit significant jumps linked to changes of mineralogy and/or grain size of the magnetization carriers at the boundaries of zone A.

NRM/ARM varies between 0.05 and 0.28 (Fig. 6c); four intervals contain evidence of minimum NRM/ARM phases (numbered 1–4). The largest amplitude variation is recorded between 8.8 and 12 m. A decreasing trend leads to low phase 3 at 10.3 m, with a noticeable step at 8.8 m coinciding with the upper boundary of zone A. A two-fold increase including phase 4 (at 11.5 m) ends by an abrupt increase coinciding with the lower boundary of zone A. These abrupt steps are linked to mineralogical and/or grain-size changes of magnetization carriers at the boundaries of zone A. However, the continuity of NRM/ARM signal throughout zone A and throughout the adjacent sedimentary units suggests that the NRM/ARM ratio is the most appropriate proxy for the RPI variations.

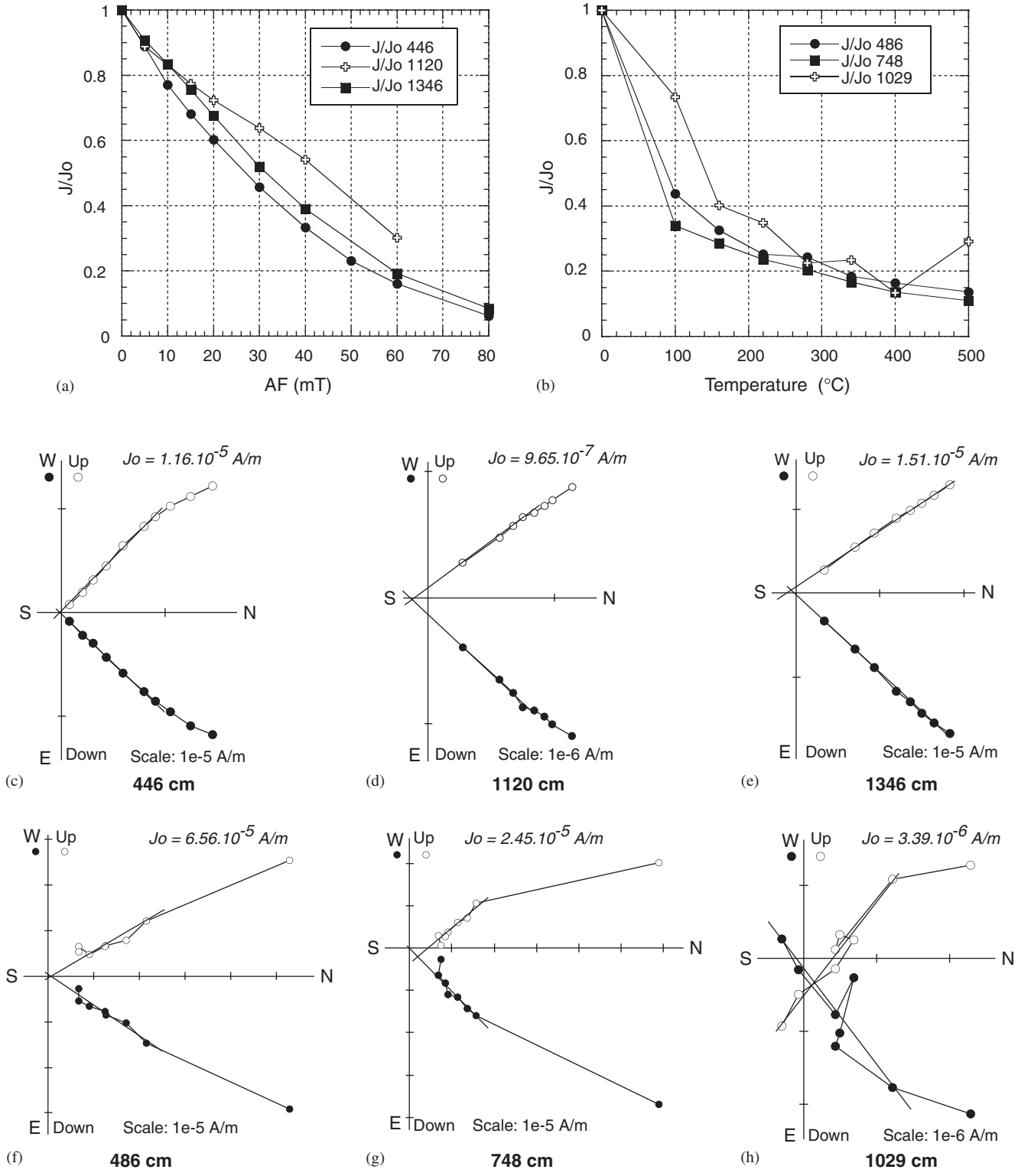

Fig. 5. AF and thermal demagnetization of selected specimens: (a, b) intensity diagrams (J/J_0), (c–e) NRM orthogonal AF demagnetization diagrams, (f–h) NRM orthogonal thermal demagnetization diagrams. Vertical component (white dots), horizontal component (black dots). The direction of the characteristic RM (straight lines) was determined from at least five steps. J_0 values and axis scales are provided in A/m.

Finally, the variations of directions and RPI are compatible with the record of regular PSV, except in the interval 10–11.5 m where large amplitude directional swings occur during a two-fold low RPI phase.

6. Chronological reconstruction and timing of the paleomagnetic variations

The chronology of the sequence is based on 12 ^{14}C ages corrected for a 400-year reservoir effect and calibrated

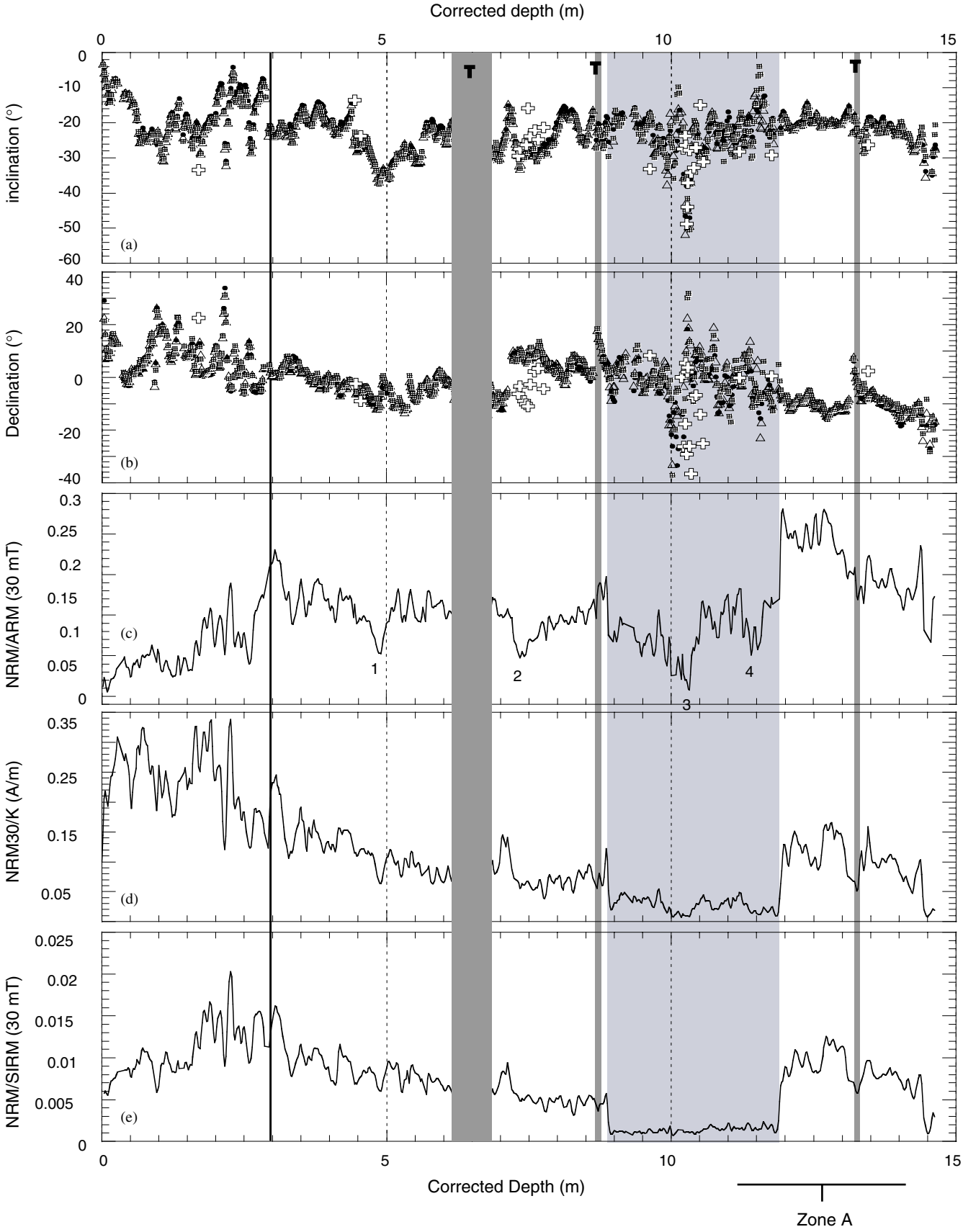

Fig. 6. Directions and normalized NRM intensity measured on U-channels and on discrete samples plotted on the corrected depth scale (m). Data obtained in the upper 3 m, isolated by a black vertical line, are not considered in the text. Data obtained from the pristine tephra layer (6–7 m) are hidden behind a grey band (see text). (a) Inclination and (b) declination at AF steps: black dots (20 mT), white triangles (30 mT), grey squares (40 mT); white crosses for discrete samples directions. Normalized NRM intensity obtained from three parameters: (c) NRM_{30}/ARM_{30}, (d) NRM_{30}/K (A/m), (e) $NRM_{30}/SIRM_{30}$. A light-grey band underlines zone A. The NRM_{30}/ARM_{30} considered as RPI index contains four low-RPI intervals labelled 1–4.

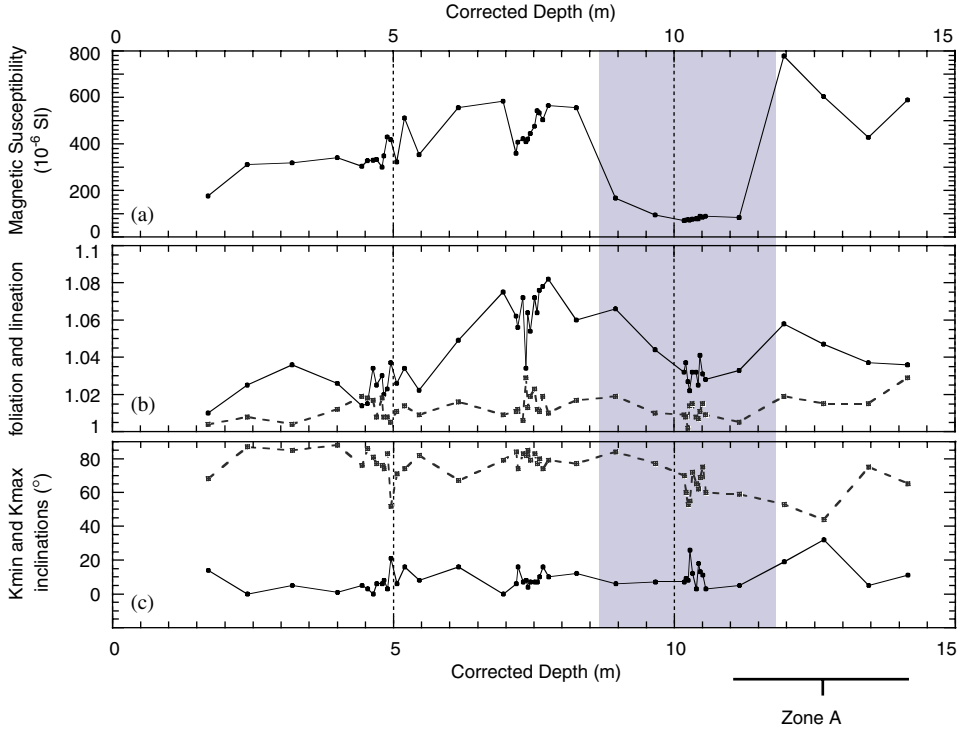

Fig. 7. Anisotropy of MS parameters plotted on the corrected depth (m). (a) MS of the selected specimens, (b) foliation (full line and black dots), lineation (broken line and grey squares), (c) K_{min} (broken line and grey squares), K_{max} inclinations (full line and black dots). The sampling resolution was increased in the layers carrying anomalous paleomagnetic signatures. A light-grey band underlines zone A.

Table 1
Calibrated ^{14}C ages (De Garidel-Thoron et al., 2004) used to construct the age-depth model of core MD97-2134

Corrected depth (m)	Calibrated ^{14}C age (ka BP)	1 sigma error (ka)
0	0.418	0.06
0.09	0.768	0.06
0.86	3.844	0.06
1.3	5.407	0.07
1.66	8.082	0.07
2	8.502	0.08
2.93	11.501	0.09
3.34	13.822	0.09
3.58	16.233	0.11
4.58	26.463	0.19
4.92	32.125	0.31
5.67	34.628	0.34
6.2	36.066	0.37

Ages were corrected from a 400 yrs reservoir age, and calibrated using Stuiver et al. (1998) and Bard (1998) methods.

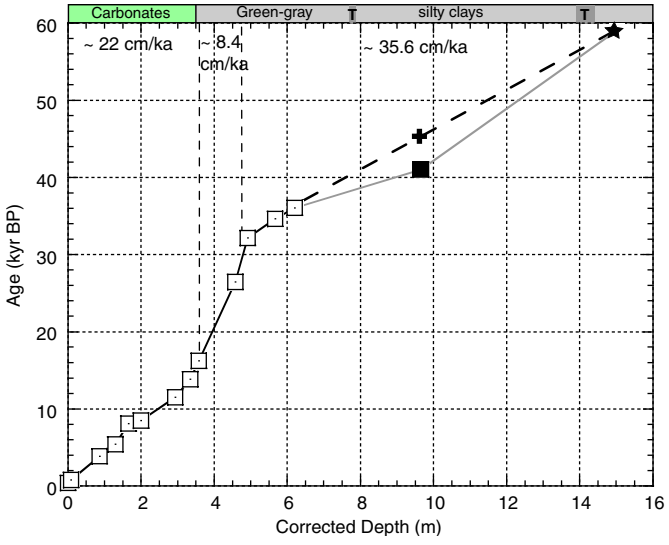

Fig. 8. Chronological data and age/depth relationship used to construct the core time scale. The depth scale is corrected by removal of the 66 cm pristine tephra (see text). Radiocarbon ages (13 data given in Table 1) are represented by white squares including the 1σ error bars. The MIS 3/4 boundary is represented by a black star. The stratigraphic position of the paleomagnetic anomaly is presented as a cross (linear interpolation) and a black square (tuned chronology considering its identification with the Laschamp excursion dated at 41 ka BP). Sedimentation rates are indicated.

using INTCAL 1998 (Stuiver et al., 1998) for the last 20 ka and the equation proposed by Bard (1998) beyond 25 ka BP (Table 1 and Fig. 8). The oldest chronological tie-point is 59 ka BP and corresponds to the transition from the MIS 4 to 3 (Martinson et al., 1987) identified in the δ^{18}O record of planktic foraminifera *Globigerinoides ruber* (De Garidel-Thoron et al., 2004).

After removal of the 66 cm thickness of the pristine tephra inter-bedded at ~6.8 m, considered as an instantaneous deposit, we constructed the age model by applying a linear interpolation between the successive tie-points (Fig. 8). Based on this age model, the major paleomagnetic

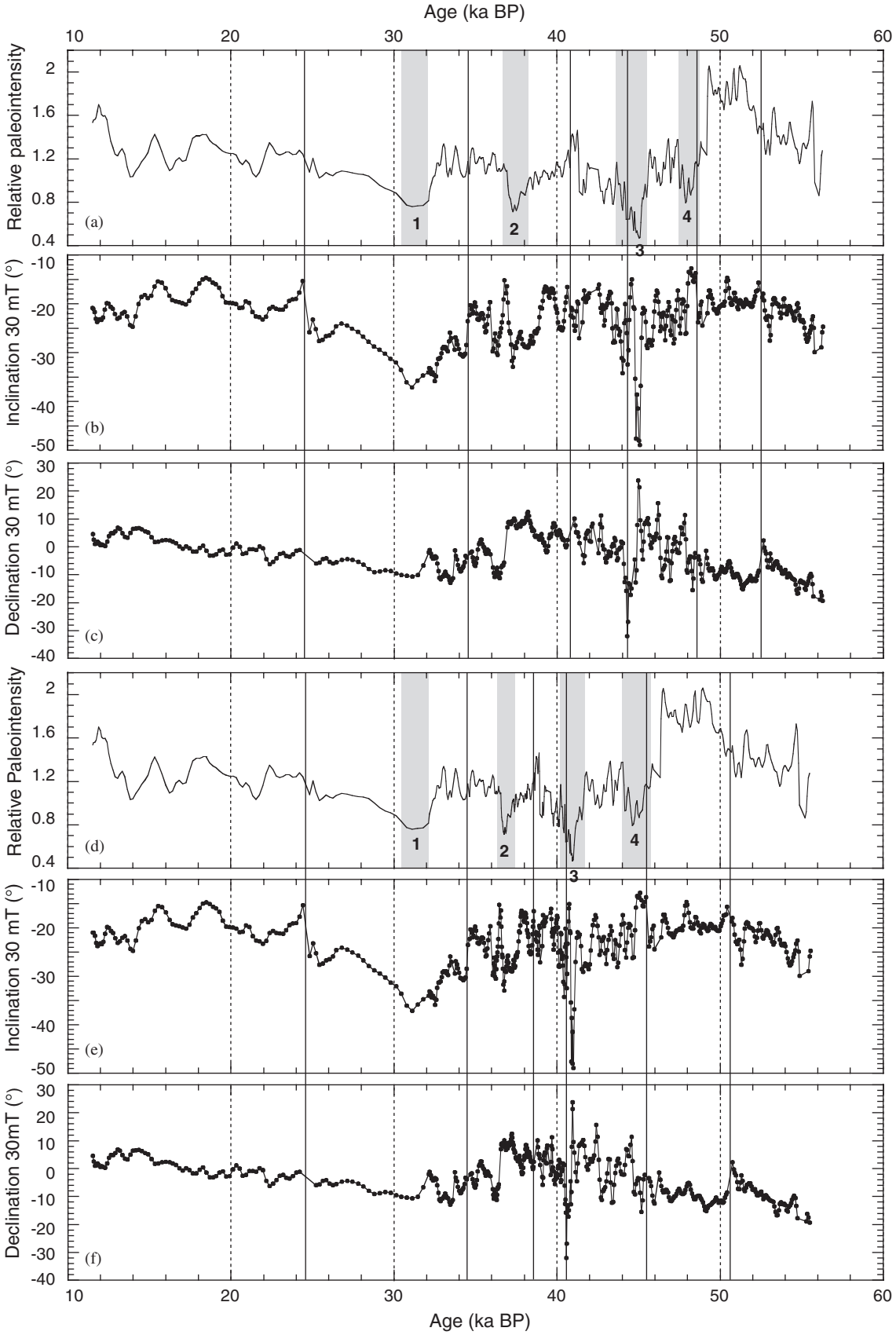

Fig. 9. Paleomagnetic record presented on two time scales version: (a–c) first interpolated time scale (see text for details), (d–f) tuned time scale using the 41 ka BP age as a tie point. (a, d) RPI: normalized NRM_{30}/ARM_{30} values (i.e. divided by the average value computed over the whole record), (b, e) inclination at 30 mT and (c, f) declination at 30 mT. Thin black lines indicate the position of sections limits. Low RPI intervals are labelled 1–4.

features occurred at 31, 37, 45 and 48 ka BP coinciding, respectively, with RPI lows 1, 2, 3 and 4 (Fig. 9a–c). The directional anomaly characterized by highly negative inclinations and eastward declinations is dated at 45 ka BP, and corresponds to the weak RPI low 3. This event is rapidly followed by a return to low negative inclinations accompanied by a westward declination swing. We interpret such a large-scale directional behaviour during a low RPI event as the expression of a smoothed excursion. The geomagnetic excursion classically reported worldwide in the 45–40 ka BP time period is the Laschamp excursion, dated at 40.4 ± 2 ka BP by Ar/Ar (Guillou et al., 2004), and not significantly different from the age of 41 ka BP retained in both NAPIS (Laj et al., 2000) and SAPIS (Stoner et al., 2002) reconstructions.

The accuracy of the chronological reconstruction can be discussed on the ground of this identification. The depth–age function can be improved by adding the age of the Laschamp excursion as a tie-point (41 ka BP at 10.3 m depth). This solution introduces a minor change of apparent sedimentation rates (Fig. 8) in comparison with those occurring at 3.5 and 5 m depths. The age of the older RPI events is thus significantly modified: low RPI event 3 naturally falls at 41 ka BP and the low RPI event 4 now falls at 45 ka BP (from 48 ka BP). Low-RPI events 1 and 2 are tightly constrained by ^{14}C ages at ~31 and ~37 ka BP, respectively. Despite the absence of concomitant excursional directions, it is possible to propose a correlation of these low RPI events with the events of weak dipole moment linked to the Mono Lake excursion and to the late part of the Laschamp excursion introduced by Negrini et al. (2000).

7. Discussion

In order to assess the validity of the RPI curve on its tuned chronological scale, we compared it with paleointensity stacks reconstructed for the North Atlantic (NAPIS) and South Atlantic (SAPIS) regions (Fig. 10). These stacks were recently completed with new individual records and merged as a global paleointensity stack (GLOPIS) (Laj et al., 2004). When separately plotted, however, NAPIS and SAPIS still present significant differences in the amplitude and in the structure of the RPI, decrease from ~50 to 40 ka BP. SAPIS is characterized by a smaller amplitude and by an additional RPI low at 45 ka BP. A second difference is the timing and structure of the RPI lows recorded after 33 ka BP; i.e. the youngest RPI low is shifted by 3–4 ka.

The timing and structure of RPI lows in the MD97-2134 record better agrees with the SAPIS succession, but it must be emphasized that the larger shifts between the MD97-2134 and NAPIS records may partially be explained by different chronological constraints (^{14}C ages and SPECMAP for MD97-2134 and tuning on GISP2 for NAPIS-75).

Finally, the comparison presented in Fig. 10 suggests a reasonable coherency between the MD97-2134 record with

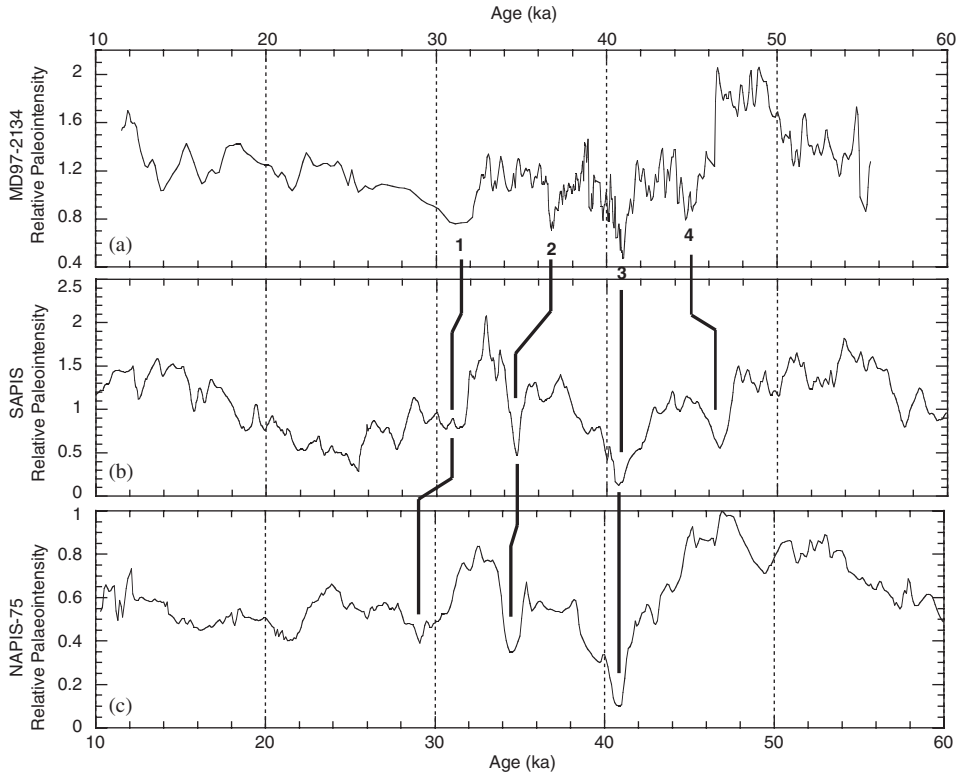

Fig. 10. Comparison of the MD97-2134 RPI record (a) with the SAPIS (b) and NAPIS and (c) RPI stacks. Correlations of major features 1–4 are underlined.

the SAPIS record, but to a lesser extent with the NAPIS record, over the interval 30–50 ka BP.

A detailed study of the authigenic $^{10}Be/^{9}Be$ ratio across the 25–55 ka BP interval (Leduc et al., 2004) has been performed in order to assess the reliability of the RPI record (Elsasser et al., 1956; Lal, 1988; Carcaillet et al., 2004). Three significant peaks of the authigenic $^{10}Be/^{9}Be$ ratio confirm the overproduction of the cosmogenic nuclide at the time of low-RPI events 1, 2 and 3. Low-RPI event 4 does not seem to be deep enough to induce a significant overproduction. Surprisingly, the largest $^{10}Be/^{9}Be$ peak is not correlated with the most severe low-RPI event 3, assigned to the Laschamp excursion (41 ka BP), but is coeval with the low-RPI event 2 dated at 37 ka BP. These results will be presented in detail and discussed in the light of the paleomagnetic results in another article. They support our paleomagnetic results introducing a complex behaviour of the geomagnetic field, with 3 major and one minor events of weak dipole moment between 30 and 50 ka BP.

Acknowledgements

We thank Luc Beaufort, Chief of the IMAGE II "IPHIS" coring campaign, Yvon Balut, Chief of the operation on board of the *R.V. Marion Dufresne* and the I.P.E.V. (Institut Paul-Emile Victor). We thank Pierre Rochette, David Williamson and Pierre-Etienne Mathé for fruitful discussion. Two anonymous reviewers as well as Professor Jim Rose, Editor in chief of QSR, helped to improve the quality of this manuscript.

References

Bard, E., 1998. Geochemical and geophysical implications of the radiocarbone calibration. Geochemica and Cosmochemica Acta 62, 2025–2038.

Benson, L., Liddicoat, J.C., Smoot, J., Sarna-Wojcicki, A., Negrini, R., Lund, S., 2003. Age of the Mono Lake excursion and associated tephra. Quaternary Science Reviews 22, 135–140.

Bonhommet, N., Babkine, J., 1967. Sur la présence d'aimantations inverses dans la Chaine des Puys, Massif Central (France), p. 92.

Bonhommet, N., Zahringer, J., 1969. Paleomagnetism and potassium argon age determinations of the Laschamp geomagnetic polarity event. Earth and Planetary Science Letters 6, 43–46.

Carcaillet, J., Bourles, D.L., Thouveny, N., Arnold, M., 2004. An authigenic 10-Be/9-Be record of geomagnetic moment variations and excursions over the last 300 ka. Earth and Planetary Science Letters 219, 397–412.

Channell, J.E.T., Stoner, J.S., Hodell, D.A., Charles, C.D., 2000. Geomagnetic paleointensity for the last 100 kyr from the sub-antartic South Atlantic: a tool for inter-hemispheric correlation. Earth and Planetary Science Letters 175, 145–160.

Cogné, J.P., 2003. PaleoMac: a Macintosh™ application for treating paleomagnetic data and making plate reconstructions. Geochemistry Geophysics Geosystems 4 (1), 1 CiteID 1007.

De Garidel-Thoron, T., Beaufort, L., Bassinot, F.C., Henry, P., 2004. Evidence for large methane releases to the atmosphere from deep-sea gas-hydrates dissociation during the last glacial episode. Proceedings of the National Academy of Sciences of the United States of America 101, 9187–9192.

Denham, C.R., Cox, A., 1971. Evidence that the Laschamp polarity event did not occur 13300–30400 years ago. Earth and Planetary Science Letters 13, 181–190.

Elsasser, W., Ney, E.P., Winckler, J.R., 1956. Cosmic-ray intensity and geomagnetism. Nature 178, 1226–1227.

Gillot, P.Y., Labeyrie, J., Laj, C., Valladas, G., Guerin, G., Poupeau, G., Delibrias, G., 1979. Age of the Laschamp geomagnetic polarity excursion revisited. Earth and Planetary Science Letters 42, 444–450.

Guillou, H., Singer, B., Laj, C., Kissel, C., Scaillet, S., Jicha, B.R., 2004. On the age of the Laschamp geomagnetic excursion. Earth and Planetary Science Letters 227, 331–343.

Kent, D.V., Hemming, S.R., Turrin, B.D., 2002. Laschamp excursion at Mono Lake? Earth and Planetary Science Letters 6121, 1–14.

King, J.W., Banerjee, S.K., Marvin, J., 1983. A new rock magnetic approach to selecting sediments for geomagnetic paleointensity studies: application to paleointensity for the last 4000 years. Journal of Geophysical Research 88, 5911–5921.

Laj, C., Kissel, C., Mazaud, A., Channel, J.E.T., Beer, J., 2000. North Atlantic paleointensity stack since 75 ka (NAPIS-75) and the duration of the Laschamp event. Philosophical Transactions of the Royal Society of London 358, 1009–1025.

Laj, C., Kissel, C., Beer, J., 2004. High resolution global paleointensity stack since 75 kyr (GLOPIS-75) calibrated to absolute values. In: Timescales of the Paleomagnetic Field. Geophysical Monograph Series, vol. 145, pp. 255–265.

Lal, D., 1988. Theoretically expected variations in the terrestrial cosmic-ray production rates of isotopes. In: Castagnoli, G.C., Lal, D. (Eds.), Solar-Terrestrial Relationships. Soc. Italiana di Fisica-Bologna-Italy, Bologna, pp. 216–233.

Leduc, G., Thouveny, N., Bourlès, D.L., Blanchet, C., Carcaillet J., 2004. Authigenic $^{10}Be/^{9}Be$ recorded in western Equatorial Pacific sediments over the Laschamp and Mono lake excursions. Implication for cosmonuclide production rates. Eos Transactions AGU 85(47); Fall Meet, Supplement, Abstract GP 43B-0859.

Liddicoat, J.C., 1992. Mono lake excursion in Mono Basin, California, and at Carson Sink and Pyramid Lake, Nevada. Geophysical Journal International 108, 442–452.

Liddicoat, J.C., 1996. Mono lake excursion in the Lahontan Basin, Nevada. Geophysical Journal International 125, 630–635.

Liddicoat, J.C., Coe, R.S., 1979. Mono Lake geomagnetic excursion. Journal of Geophysical Research 84, 261–271.

Martinson, D.G., Pisias, N.G., Hays, J.D., Imbrie, J., Moore, T.C., Shackelton, N.J., 1987. Age dating and the orbital forcing theory of the Ice Ages: development of a Height-Resolution 0 to 300,000 year chronostratigraphy. Quaternary Research 27, 1–29.

Mazaud, A., Sicre, M.A., Ezat, U., Pichon, J.J., Duprat, J., Laj, C., Kissel, C., Beaufort, L., Michel, E., Turon, J.L., 2002. Geomagnetic-assisted stratigraphy and sea surface temperature changes in core MD94-103 (Southern Indian Ocean): possible implications for North–South climatic relationships around H4. Earth and Planetary Science Letters 201, 159–170.

Negrini, R.M., Davis, J.O., Verosub, K.L., 1984. Mono Lake geomagnetic excursion found at Summer Lake, Oregon. Geology 12, 643–646.

Negrini, R., Erbes, K.F., Herrera, A.M., Roberts, A.P., Cohen, A., Palacios-Fest, M., Wigand, P.E., Foit, F., 2000. A paleoclimate record for the past 250,000 years from Summer Lake, Oregon, USA: I. Age control and magnetic lake level proxies. Journal of Paleolimnology 24, 125–149.

Peters, C., Thompson, R., 1998. Magnetic identification of selected natural iron oxides and sulphides. Journal of Magnetism and Magnetic Material 183, 365–374.

Roberts, A.P., 1995. Magnetic properties of sedimentary greigite (Fe_3S_4). Earth and Planetary Science Letters 134, 227–236.

Rochette, P., Vadeboin, F., Clochard, L., 2001. Rock magnetic applications of Halbach cylinders. Physics of the Earth and Planetary Interiors 126, 109–117.

Roperch, Y., Bonhommet, N., Levi, S., 1988. Paleointensity of the Earth's magnetic field during the Laschamp excursion and its geomagnetic implications. Earth and Planetary Science Letters 88, 209–219.

Stoner, J.S., Laj, C., Channell, J.E.T., Kissel, C., 2002. South Atlantic and North Atlantic geomagnetic paleointensity stacks (0–80 ka): implications for inter-hemispheric correlations. Quaternary Science Review 21, 1141–1151.

Stuiver, M., Reimer, P.J., Bard, E., Beck, J.W., Burr, G.S., Hughen, C.A., Kromer, B., McCormac, G., Van Der Plicht, J., Spurk, M., 1998. INTCAL98 radiocarbon age calibration, 24,000–0 cal BP. Radiocarbon 40, 1041–1083.

Tauxe, L., 1993. Sedimentary records of relativre paleointensity of the geomagnetic field: theory and practice. Review of Geophysics 31, 319–354.

Thouveny, N., Creer, K.M., Blunk, I., 1990. Extension of the Lac du Bouchet palaeomagnetic record over the last 120,000 years. Earth and Planetary Science Letters 97, 140–161.

Thouveny, N., Creer, K.M., Williamson, D., 1993. Geomagnetic moment variations in the last 70,000 years, impact on production of cosmogenic isotopes. Global and Planetary Change 7, 157–172.

Thouveny, N., Carcaillet, J., Moreno, E., Leduc, G., Nérini, D., 2004. Geomagnetic moment variation and paleomagnetic excursions since 400 ka BP: a stacked record of sedimentary sequences of the Portuguese margin. Earth and Planetary Science Letters 219, 377–396.

Vlag, P., Thouveny, N., Williamson, D., Rochette, P., Ben Atig, F., 1996. Evidence for a geomagnetic excursion recorded in the sediments of Lac St Front, France: a link with the Laschamp excursion? Journal of Geophysical Research 101, 28211–28230.

Wagner, G., Beer, J., Laj, C., Kissel, C., Masarik, J., Muscheler, R., Synal, H.-A., 2000. Chlorine 36 evidence for the Mono Lake event in the summit GRIP ice core. Earth and Planetary Science Letters 181, 1–6.

Zic, M., Negrini, R., Wigand, P.E., 2002. Evidence of synchronous climate change across the Northern Hemisphere between the North Atlantic and the northwestern Great Basin, United States. Geology 30, 635–638.